EFFECT OF DEPOSITION TIME ON THE STRUCTURAL AND OPTICAL PROPERTIES OF MOLYBDENUM CHALCOGENIDES THIN FILMS

S. SHARIZA AND T. JOSEPH SAHAYA ANAND[*]
Department of Engineering Materials, Faculty of Manufacturing Engineering, Universiti Teknikal Malaysia Melaka, Durian Tunggal, 76100 Melaka, Malaysia

Molybdenum chalcogenides, specifically molybdenum selenide, $MoSe_2$ and molybdenum sulphide, MoS_2 thin films have been successfully deposited onto indium-tin-oxide (ITO) coated glass substrates and stainless steel substrates by electrodeposition technique. The effects of the deposition time on the growth, structural and optical properties of the films were then studied. X-ray diffraction (XRD) patterns have confirmed the polycrystalline rhombohedral $MoSe_2$ and hexagonal MoS_2 phase formation. The results show that the intensity of XRD peaks for these materials increases with the increase of deposition time. UV -VIS spectrophotometric measurement revealed that the optical band gap values of the thin films decreased with the increase of deposition time and lie in the range from 1.12 – 1.22 eV for $MoSe_2$ and 1.65 – 1.74 eV for MoS_2 thin films. Surface morphology studies by scanning electron microscopy showed uniform and continuous thin film with layered structure surface.

1. Introduction

The preparation of thin film materials opens the opportunity of observing the evolution of physical properties of the materials with sizes [1]. The reduction of sizes, in terms of thickness of the thin film provide the possibility of observing novel behaviours such as size dependent structural, electrical and optical properties [2]. Concurrently, the preparation of transition metal chalcogenides (TMC) has been done extensively for its high potential use in the non-conventional energy resources industries [3-4]. In recent years, TMC compounds such as CdHgSe, $ZrSe_2$, CdSeTe, WSSe, and CdS have been actively investigated for photoelectrochemical (PEC) and solar cell applications [5-9].

Generally, TMC compounds can be obtained in thin film form by various methods, including sputtering [2], chemical bath deposition [10], selenization [13], solid state reaction [14], sulphurization [15] and electrolytic reduction [16]. However, they are cost intensive and sometimes present special problems for the preparation of transition metal chalcogenide films [17]. Aside from this, the electrodeposition method offers simplicity and economy, control of film thickness, uniformity and possibility of deposition of thin films onto substrates of large and complex shape [18].

In this paper, the electrodeposition technique at potentiostatic mode for depositing molybdenum chalcogenide thin films cathodically on both ITO–coated conducting glass substrates as well as stainless steel substrates is presented. The various aspects of thin films like growth mechanism, characterization and some of its properties are discussed.

---

[*] Corresponding author: anand@utem.edu.my

2. Experimental details

2.1 Electrodeposition of molybdenum chalcogenide thin films

The electrodeposition of the molybdenum chalcogenide (both $MoSe_2$ and MoS_2) thin films was carried out using a Princeton Applied Research Model VersaSTAT 3 Potentiostat. The deposition potential of the molybdenum chalcogenide thin film was first derived from cyclic voltammetry (CV) technique followed by synthesis of the chalcogenides by electrodeposition technique.

A three – electrode cell system was adopted for the cyclic voltammetry analysis and deposition of the film as shown in Fig. 1. The electrolysis cell consisted of (i) an ITO-coated glass substrate or stainless steel substrate as the working electrode (WE) on which the molybdenum chalcogenide thin film is to be deposited; (ii) graphite as the counter electrode (CE); and (iii) a saturated calomel electrode (SCE) with Ag/AgCl reference system as the reference electrode [19]. The SCE measures the potential of the working electrode. The electrode spacing should be carefully adjusted to obtain good results. Both working and counter electrodes are kept as close as 1 cm to each other and the two surfaces facing each other were kept parallel, so that released ions will be attracted and deposited exactly perpendicular to the cathode surface. The reference electrode tip is placed very close to the cathode surface so that the exact potential at the surface will be monitored unaffected by the solution resistance (internal resistance of the cell).
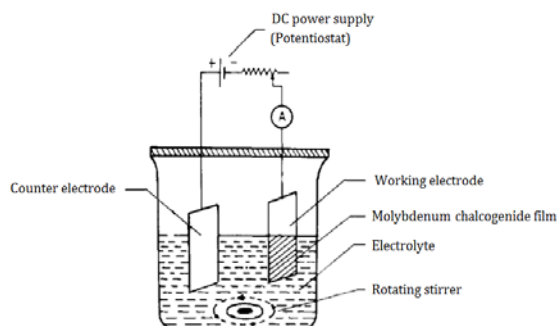

Fig. 1. Electrolysis cell setup for molybdenum chalcogenide thin film deposition.

For the deposition of molybdenum selenide, $MoSe_2$ and molybdenum sulphide, MoS_2 thin films, an ammoniacal solution consisting of a mixture of molybdic acid and selenium dioxide ($H_2MoO_4 + SeO_2$) and molybdic acid and sodium thiosulphate pentahydrate ($H_2MoO_4 + Na_2S_2O_3.5H_2O$) was used as electrolyte, respectively. The deposition of films was carried out at a temperature of 40 ± 1 °C for 30 minutes. To prepare electrolyte solutions having relative concentrations of H_2MoO_4 and SeO_2, the following two basic solutions were first prepared: solution A containing H_2MoO_4 in ammonia and solution B containing SeO_2 in water. Equal volumes of these two basic solutions were mixed to obtain the electrolysis solutions. The similar procedure was followed for the electrolyte solutions of H_2MoO_4 and $Na_2S_2O_3.5H_2O$.

2.2 Characterization of thin films

The X-ray diffractograms of the thin film was obtained on a PANalytical XPERT PROMPD PW 3040/60 diffractometer using monochromatic CuK_α radiation ($\lambda = 1.5405$ Å) in the range of 2θ angles from $10 – 90°$. The metal chalcogenide's crystallographic properties such as the crystal system, 'd' spacing values and (*hkl*) planes were analyzed. The optical absorption spectrum studies were carried out in the wavelength range 200 to 1100 nm at room temperature using a Shimadzu 1700 UV-Vis Spectrophotometer. The surface morphological studies were conducted on a JSM 6400 JOEL scanning electron microscope (SEM). This study will reveal the uniformity of the surface area of the electrodeposited thin film.

3. Results and discussion

3.1 Electrodeposition and physical properties of films

Cyclic voltammetry (CV) test was carried out before the deposition process. It was done between two potential limits (-1.00 V to 1.00 V) for the solutions prepared to probe the prospective potentials for deposition of the thin films. The solutions are those of the mixture of ammoniacal H_2MoO_4 + SeO_2 (solution A) and the mixture of ammoniacal H_2MoO_4 + $Na_2S_2O_3.5H_2O$ (solution B) for the deposition of $MoSe_2$ and MoS_2, respectively. The Electrochemical Analysis System Software (PAR Versa Studio 2.0) was used to control the deposition process and to monitor the current and voltage profiles.

Fig. 2 and 3 shows the cyclic voltammogram of the electrodes in solutions A and B for $MoSe_2$ and MoS_2, respectively. As shown in Fig. 2, the forward scan almost immediately dropped and remained constant until a current drop at -0.5 V suggesting a reduction process. The current change is associated with the reduction of molybdenum and selenide ions to form solid molybdenum selenide, $MoSe_2$ compound on the substrate. The deposition of molybdenum selenide on the substrate continued until the equilibrium potential is achieved at an interception between the forward and reverse scan at approximately -0.1 V versus Ag/AgCl.
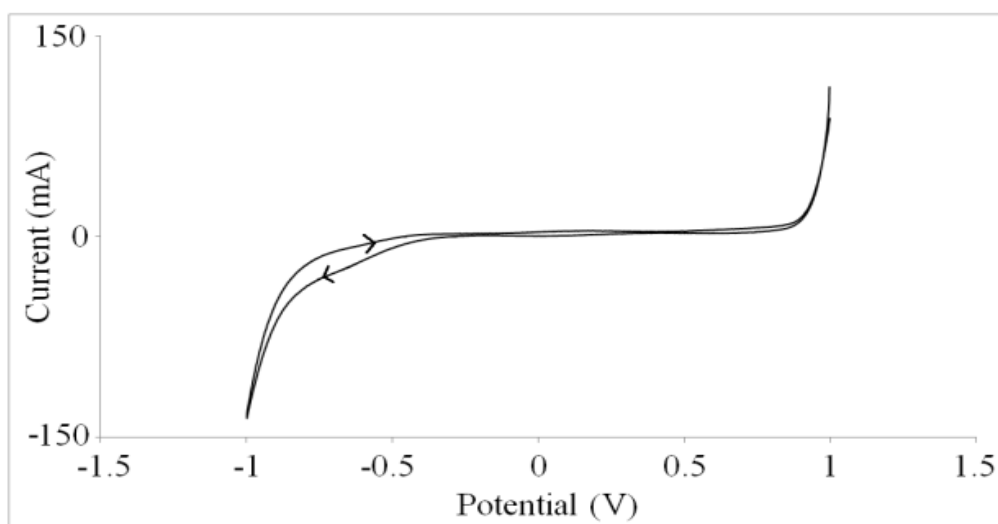

Fig. 2. Cyclic voltammogram of the electrodes in ammoniacal H_2MoO_4 + SeO_2 solution

As for the cyclic voltammetry measurements of MoS_2 deposition shown in Fig. 3, the forward scan initially dropped and remained constant until a current drop at -0.8 V suggesting a reduction process (See inset figure). Similarly as stated before, the current change is associated with the reduction of molybdenum and sulphide ions to form solid molybdenum sulphide, MoS_2 compound on the substrate. The deposition of molybdenum sulphide on the substrate continued until all the equilibrium potential is achieved at an interception between the forward and reverse scan at approximately 0.1 V versus Ag/AgCl.
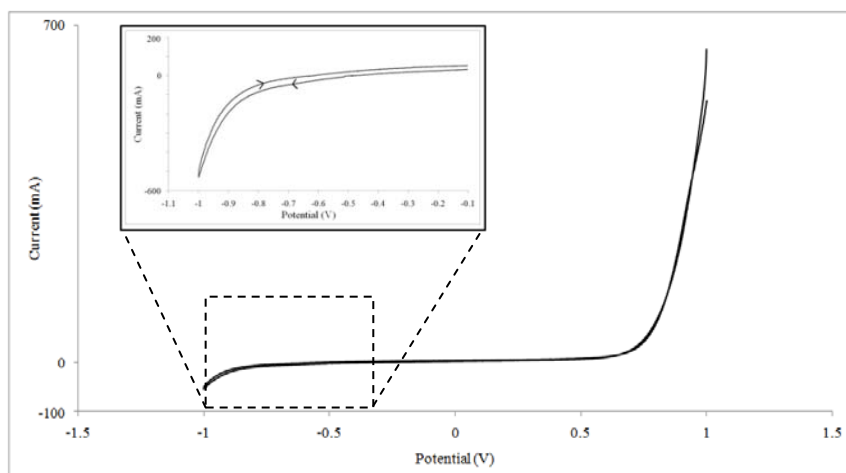
532

Fig. 3. Cyclic voltammogram of the electrodes in ammoniacal H_2MoO_4 + $Na_2S_2O_3.5H_2O$ solution.

From the results obtained through CV measurements of the system, the deposition of $MoSe_2$ and MoS_2 thin films on ITO-coated glass substrates and stainless steel substrates were carried out at the selected potential -1.0 *V* versus Ag/AgCl. The deposition temperature of the thin films were set and controlled at 40 °C ± 1 °C while the deposition time of the thin films was set at 10, 15, 20, 25 and 30 minutes for both compounds.

From the above reactions, it appears that an increase in the film thickness is expected as the deposition times are increased. A plot of thickness versus deposition times for both types of films is displayed in Fig. 4. The thickness of the thin films were calculated by using the relation between mass and volume in the density calculation, where density is equal to the value of mass over the volume as in equation below.

$$\text{Thickness (cm)} = \frac{\text{Mass (g)}}{\text{Density (g/cm}^3) \times \text{Area (cm}^2)}$$

The growth shows an initial induction period of about 10 minutes, in this period, a very thin, almost no film formation, and thereafter, the film begins to form. The presence of initial induction period can be attributed to the growth mechanism where nucleation occurs first followed by the combination of ions for the film growth.
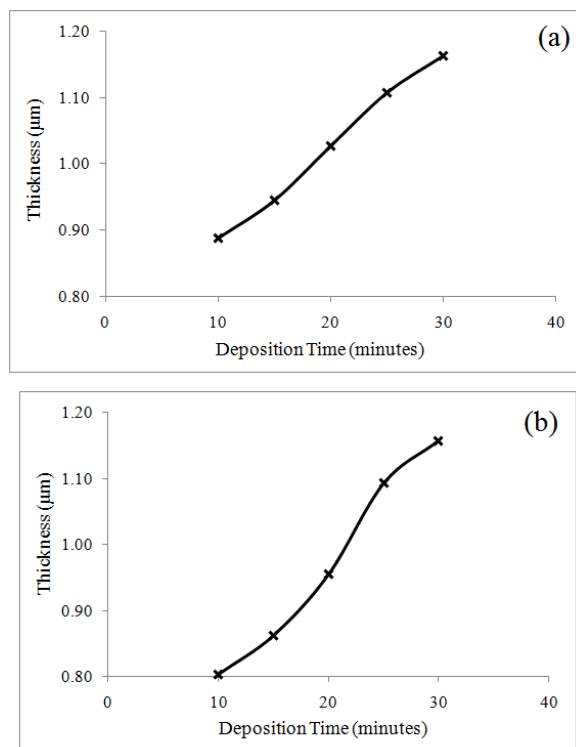
Fig. 4. Variation of thickness with deposition time for (a) MoSe₂, (b) MoS₂ films

3.2 Structural Characterization

X-ray diffraction (XRD) patterns of the electrodeposited molybdenum selenide, $MoSe_2$ and molybdenum sulphide, MoS_2 thin film on stainless steel substrate is shown in Fig. 5 and 6. Films on stainless steel substrates were characterized for XRD due to the amorphous feature that was obtained when characterizing the films on ITO-coated glass substrates. XRD peaks, identified in the figure, have been indexed with the help of the Joint Committee of Powder Diffraction Standards (JCPDS) file and the corresponding XRD data values are summarized in Table 1 and 2 for $MoSe_2$ and MoS_2 thin films, respectively.

The XRD analysis reveals that $MoSe_2$ films deposited on stainless steel substrates at different deposition times are polycrystalline in nature due to the sharp peaks on the XRD patterns as it can be seen in Figure 6. The peaks are identified as (101), (015), (107) and (018) planes of $MoSe_2$; and (111) and (220) planes of the stainless steel substrate [20]. The structural features fit into the rhombohedral structure of the $MoSe_2$ films with lattice parameter values $a = b = 0.3292$ nm and $c = 1.9392$ nm which is in good agreement with the standard values [21].
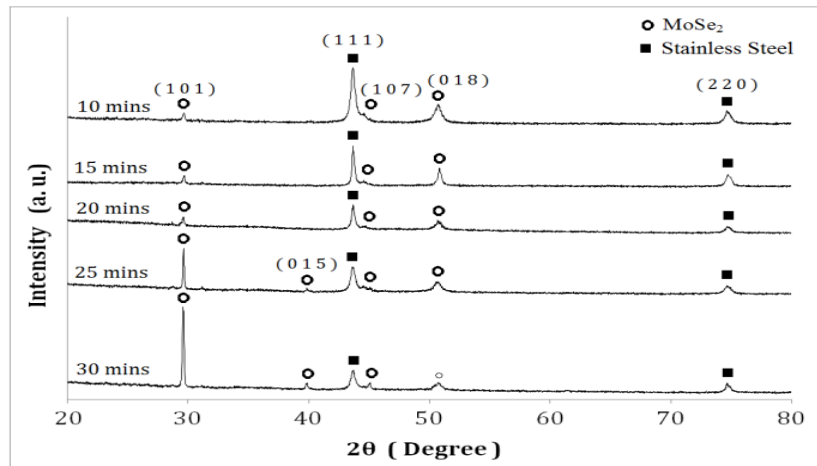
Fig. 5. X-ray diffraction pattern for MoSe₂ thin films deposited at different deposition times.

Peaks belonging to $MoSe_2$ are detected for the films prepared at all the deposition times investigated. However, it can be seen in the figure that at 10 minutes deposition time of $MoSe_2$, the peak for the stainless steel substrate are more prominent in intensity comparing to $MoSe_2$ peaks. As deposition time increase, the peaks of $MoSe_2$ especially at $2\theta = 29.5°$ and $45.1°$ become more prominent indicating that the (101) and (107) plane films grow with time. Also, at deposition time 25 minutes and 30 minutes, a $MoSe_2$ film having (015) plane structure emerges at $2\theta = 39.8°$. The stainless steel peak at $2\theta = 43.6°$ which is the most intense peak at 10 minutes have shrunk at deposition time 30 minutes due to the growth of (107) plane films which has surmount over the stainless steel peaks. As for the (018) plane structure of $MoSe_2$ at $2\theta = 50.8°$ and (220) plane structure of stainless steel at $2\theta = 74.7°$, the deposition time does not have any influence on them, as they appear as constant peaks for the thin films deposited at time 10 minutes up to 30 minutes.

The interplanar distances '*d*' corresponding to different *h k l* planes were calculated from the X-ray diffractograms and are recorded in Table 1. The crystallite size was calculated from the measurement of full-width at half-maximum (FWHM) in different X-ray peaks and values are in the range of 45 – 65 nm.

*Table 1: Comparison of experimental '*d*' values with JCPDS data for MoSe₂ thin film on stainless steel substrate with different deposition time*

Angle (2θ)	(h k l)	Standard (Å)	Experimental (Å)				
		'*d*'_JCPDS	*10 min*	*15 min*	*20 min*	*25 min*	*30 min*
31.70	(1 0 1)	2.8206	3.0153	2.8189	2.7241	2.8738	3.0231
39.19	(0 1 5)	2.2971	-	-	-	2.2634	2.2657
43.58	(1 1 1)	2.0750	2.0741	2.0260	2.0742	2.0767	2.0773
45.62	(1 0 7)	1.9868	2.0323	2.0351	2.0299	2.0340	2.0117
49.31	(0 1 8)	1.8467	1.8003	1.7968	1.8004	1.8009	1.7998
74.70	(2 2 0)	1.2697	1.2708	1.2695	1.2706	1.2709	1.2705

Fig. 6 shows the XRD patterns of MoS_2 films deposited on stainless steel substrates at different deposition times. Sharp peaks indicate that the films exhibit polycrystalline nature. The peaks are identified as (104) and (105) planes of MoS_2; and (111) and (220) planes of the stainless steel substrate [20]. The structural features fit into the hexagonal structure of the MoS_2 films with lattice parameter values $a = b = 0.3150$ nm and $c = 1.2300$ nm which is in good agreement with the standard values [22].
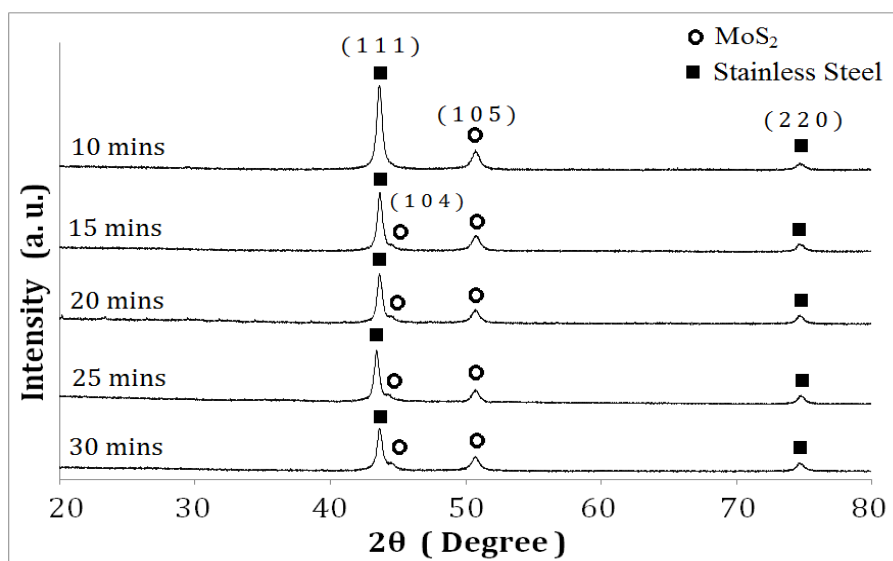
Fig. 6. X-ray diffraction pattern for MoS₂ thin films deposited at different deposition times

For MoSe₂ thin films deposited at deposition time of 10 – 30 minutes, peaks belonging to MoS₂ are detected. However, it can be seen in the figure that at 10 minutes deposition time, only one peak identified as MoS₂ peak is present at $2\theta = 50.1°$ while the peaks for the stainless steel are more visible. However, at 15 minutes deposition time, a MoS2 peak at $2\theta = 44.4°$ start to emerge and become more distinct from the neighbouring peak indicating that the (104) plane films grow with time. The stainless steel peak at $2\theta = 43.6°$ which is most intense at 10 minutes have shrunk at deposition time 30 minutes due to the growth of (104) plane films which has surmount over the stainless steel peaks. As for the (105) plane structure of MoS₂ at $2\theta = 50.1°$ and (220) plane structure of stainless steel at $2\theta = 74.7°$, the deposition time does not have any influence on the thin films, as they appear as constant peaks throughout.

Table 2: Comparison of experimental 'd' values with JCPDS data for MoS₂ thin film on stainless steel substrate with different deposition time

Angle (2θ)	(h k l)	Standard (Å)	Experimental (Å)				
		'd'$_{JCPDS}$	*10 min*	*15 min*	*20 min*	*25 min*	*30 min*
43.58	(1 1 1)	2.0750	2.0757	2.0752	2.0735	2.0738	2.0714
44.37	(1 0 4)	2.0400	-	2.0345	2.0331	2.0383	2.0334
50.08	(1 0 5)	1.8200	1.7985	1.8027	1.8017	1.7961	1.8006
74.70	(2 2 0)	1.2697	1.2707	1.2708	1.2705	1.2693	1.2705

3.3 Optical Characterization

The transition metal chalcogenides are usually indirect band gap semiconductors [23]. The optical absorption spectrum was taken for both MoSe₂ and MoS₂ thin film using an identical ITO-coated glass plate as reference. A graph of $(\alpha h v)^2$ vs. hv is drawn and the linear portion of the graph is extrapolated to the energy axis. The intercepts on the energy axis at $\alpha=0$ gives the band gaps of these compounds.

Fig. 7(a) shows the $(\alpha h v)^2$ versus hv plots of MoSe₂ thin films deposited at different deposition times (see inset graph). The variation of band gap energy (E_g) with the deposition time shows non-linear decrease is presented Fig. 7(b). It is observed that with the increase of deposition time of the films, the E_g decreased from 1.22 eV to 1.12 eV, in good E_g range with the reported value [24].

For the MoS_2 thin films, the $(\alpha h v)^2$ versus $h v$ plots of the deposited films at different deposition times is shown in Fig. 8(a) (see inset graph). Fig. 8(b) presents the non-linear decrease for the variation of band gap energy (E_g) with different deposition time. The figure shows that the E_g decreased from 1.74 eV to 1.64 eV with increase of deposition time for the MoS_2 thin films, in good range with the reported value [25].
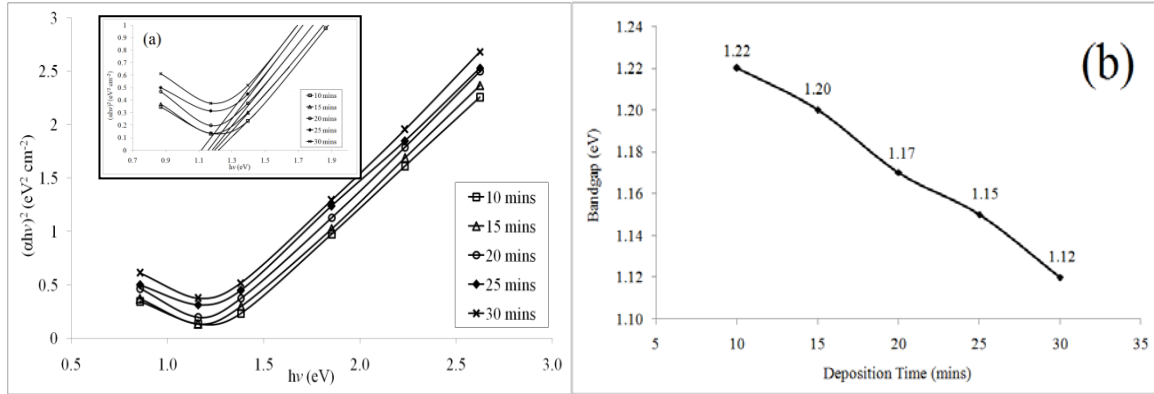

Fig. 7. Variation of MoSe₂ thin films deposited at different deposition times. (a) (αhv)² vs. hv and (b) bandgap vs.deposition time
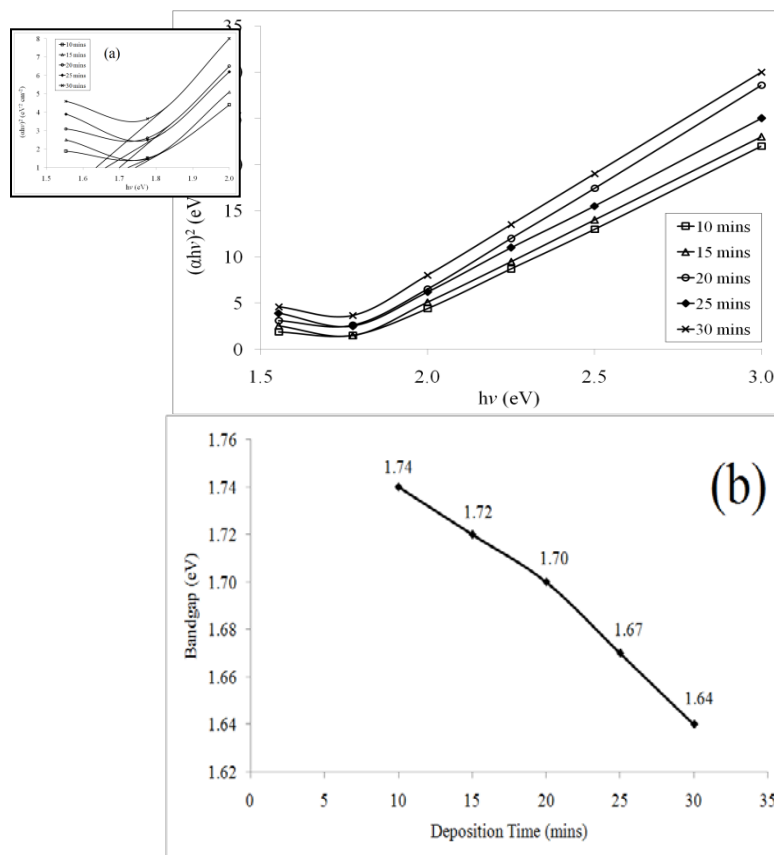

Fig. 8. Variation of MoS₂ thin films deposited at different deposition times. (a) (αhv)² vs. hv and (b) bandgap vs.deposition time

3.4 Morphological Characterization

The surface morphology of the $MoSe_2$ and MoS_2 thin films were determined by scanning electron microscope (SEM). The SEM micrograph of the $MoSe_2$ and MoS_2 thin film deposited on indium-tin-oxide (ITO) glass substrates at different deposition time is shown in Figure 9(a) - 9(c) and Figure 10(a) - 10(c).
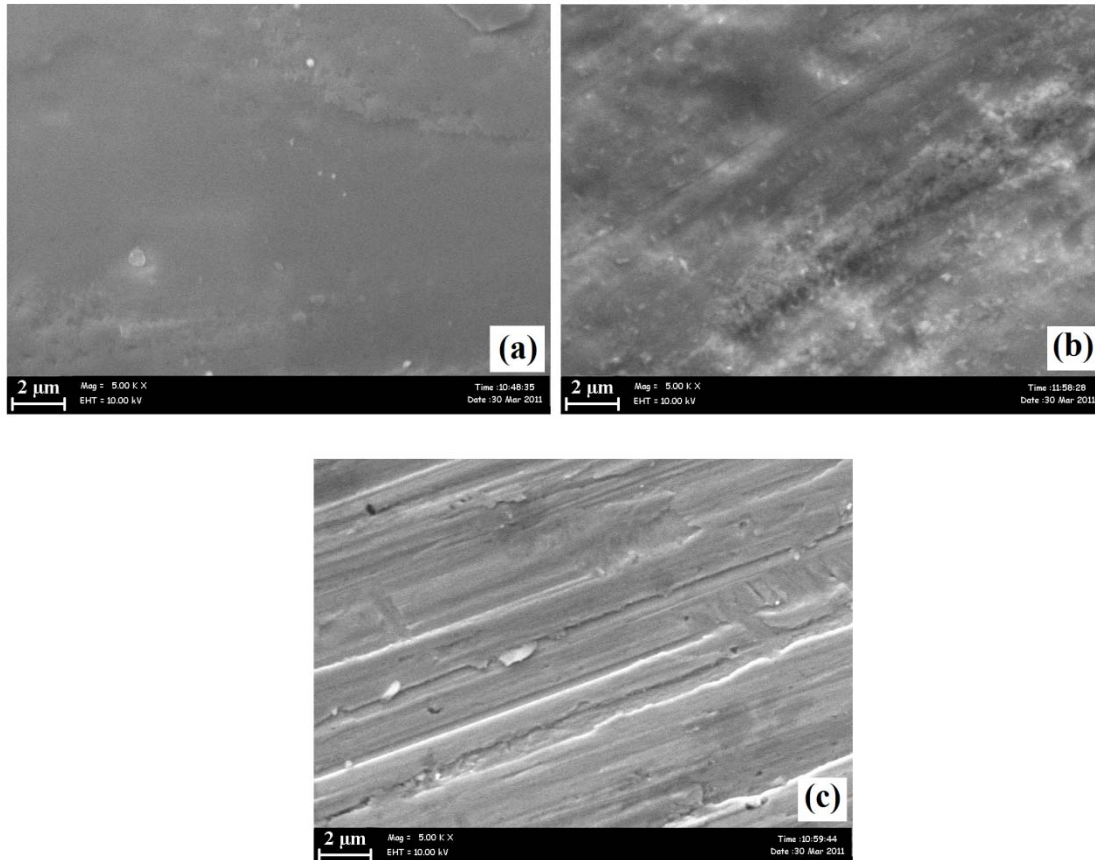

Fig. 9. Surface morphology of MoSe$_2$ thin film deposited at (a) 10 (b) 20 and (c) 30 minutes.
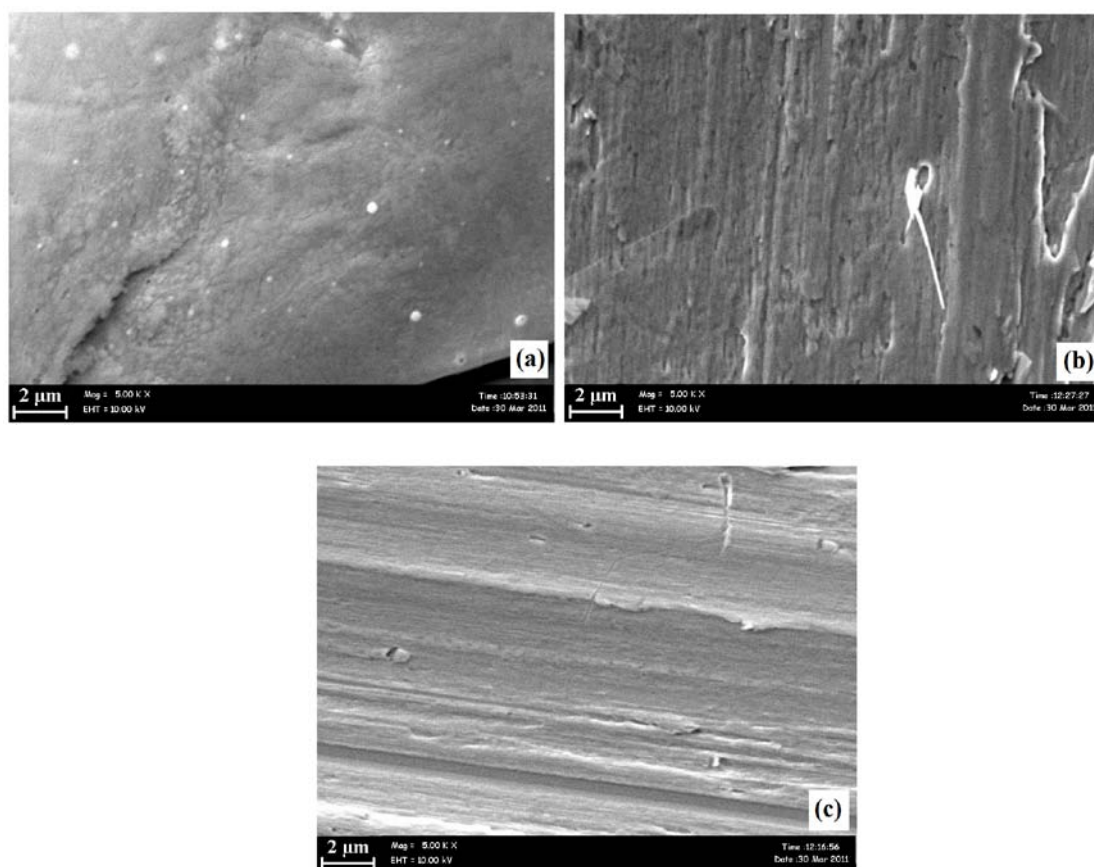
538

Fig. 10. Surface morphology of MoS₂ thin film deposited at (a) 10 (b) 20 and (c) 30 minutes

From SEM analysis, as deposition time increases, the surface of the $MoSe_2$ and MoS_2 thin films are clearly seen to be in layered structure. At deposition time 30 minutes, the surface of the thin film is found to be the best with a uniform and continuous morphology.

4. Conclusion

Using electrodeposition technique, molybdenum chalcogenide, $MoSe_2$ and MoS_2 thin films were successfully deposited on indium-tin-oxide; ITO-coated glass substrates and stainless steel substrates in which the deposition time for the thin films were optimized from 10 minutes to 30 minutes. The best stoichiometric film were deposited at an optimized deposition potential of -1.0 V_{SCE} with deposition time 30 minutes, keeping the bath at temperature 40 ± 1 °C. The XRD pattern shows that the thin films are polycrystalline in nature. The optical band energy values for the thin films were extrapolated and found to decrease with increasing deposition time. SEM photograph shows that the thin films are uniform and continuous with a layered structure for the thin films deposited at 30 minutes.

References

[1] R. S. Mane, Sankapal, B. R., Lokhande, C. D., Mater. Chem. Phys. **64**, 215 (2000).

[2] Ghosh, P. K., Ahmed, Sk. F, Saha, B., Chattopadhyay, K. K., presented at the International Workshop on Physics of Semiconductor Devices, December 16 – 20, 2007, Mumbai, India.

[3] C. Y. Cummings, G. Zoppi, Forbes, I., Dale, P. J., Scragg, J. J., Peter, L. M., Kociok-Köhn, G., Marken, F., J. Electroanal. Chem. **645**, 16 (2010).

[4] N. A.Okereke, A. Ekpunobi, J., Chalc. Lett. **8**, 377 (2011).

[5] Bhuse, V. M., Hankare, P. P., Sonandkar, S., Mater. Chem. Phys. **101**, 303 (2007).

[6] Hankare, P. P., Asabe, M. R., Kokate, A. V., Delekar, S. D., Sathe, D. J., Mulla, I. S., Chougule, B. K., J. Crys. Growth **294**, 254 (2006).

[7] Das, D., Ravi Shankar, D., Surf. Coat. Tech. **146 –147**, 498 (2001).

[8] Gujarathi, D. N., Solanki, G. K., Deshpande, M. P., Agarwal, M. K., Sol. Energy Mater. Sol. Cells **90**, 2630 (2006).

[9] Mahapatra, P. K., Dubey, A. R., Sol. Energy Mater. Sol. Cells **32**, 29 (1994).

[10] Zhang, H., Ma, X., Xu, J., Niu, J., Sha, J., Yang, D., J. Crys. Growth **246**, 108 (2002).

[11] Ghosh, P. K., Mitra, M. K., Chattopadhyay, K. K., Nanotech. **16**, 107 (2005).

[12] Huang, N. M., Radiman, S., Lim, H. N., Yeong, S. K., Khiew, P. S., Chiu, W. S., Mohamed Saeed, G. H., Nadarajah, K., Chem. Eng. J. **147**, 399 (2009).

[13] Joseph Sahaya Anand, T., Senthil, K., Electron Dev. **107**, 277 (2007).

[14] Pouzet, J., Hadouda, H., Bernede, J. C., Leny, R., J. Phys. Chem. Solids **57**, 1363 (1996).

[15] Jäger-Waldau, A., Lux-Steiner, M. Ch., Bucher, E., Scandell, L., Schumacher, A., Prins, R., App. Surf. Sc. **65-66**, 465 (1993).

[16] Ponomarev, E. A., Neumann-Spallart, M., Hodes, G., Lévy-Clément, C., Thin Sol. Films **280**, 86 (1996).

[17] Srivastava, S. K., Palit, D., Sol. St. Ionics **176**, 513 (2005).

[18] Habib M. Pathan, Sun-Ki Min, Kwang-Deog Jung, Oh-Shim Joo, Electrochem. Comm. **8,** 273 (2006).

[19] Zainal, Z., Saravanan, N., Mien, H. L., J. Mater. Sc.: Mater. in Electronics **16**, 111 (2005).

[20] JCPDS, ICDD, Card No. 33-397.

[21] JCPDS, ICDD, Card No. 1-72-1420.

[22] JCPDS, ICDD, Card No. 2-1133.

[23] Roy, P., Srivastava, S. K., Thin Sol. Films **496**, 293 (2006).

[24] Vora, M. M., Vora, A. M., Chalc. Lett **4**, 97 (2007).

[25] Patil, R. S., Thin Sol. Films **340**, 11 (1999).